An aerotaxis receptor influences invasion of *Agrobacterium tumefaciens* into its host

Zhiwei Huang [Corresp., 1] , Junnan Zou [1] , Minliang Guo [2] , Guoliang Zhang [1] , Jun Gao [1] , Hongliang Zhao [1] , Feiyu Yan [1] , Yuan Niu [1] , Guang-Long Wang [1]

[1] Jiangsu Provincial Agricultural Green and Low Carbon Production Technology Engineering Research Center, School of Life Science and Food Engineering, Huaiyin Institute of Technology, Huai'an, Jiangsu Province, China

[2] College of Bioscience and Biotechnology, Yangzhou University, Yangzhou City, Jiangsu Province, China

Corresponding Author: Zhiwei Huang
Email address: huangzhiwei@hyit.edu.cn

Agrobacterium tumefaciens is a soil-borne pathogenic bacterium that causes crown gall disease in many plants. Chemotaxis offers *A. tumefaciens* the ability to find its host and establish infection. Being an aerobic bacterium, *A. tumefaciens* possesses one chemotaxis system with multiple potential chemoreceptors. Chemoreceptors play an important role in perceiving and responding to environmental signals. However, the studies of chemoreceptors in *A. tumefaciens* remain relatively restricted. Here, we characterized a cytoplasmic chemoreceptor of *A. tumefaciens* C58 that contains an N-terminal globin domain. The chemoreceptor was designated as Atu1027. The deletion of Atu1027 not only eliminated the aerotactic response of *A. tumefaciens* to atmospheric air but also resulted in a weakened chemotactic response to multiple carbon sources. Subsequent site-directed mutagenesis and phenotypic analysis showed that the conserved residue His100 in Atu1027 is essential for the globin domain's function in both chemotaxis and aerotaxis. Furthermore, deleting Atu1027 impaired the biofilm formation and pathogenicity of *A. tumefaciens*. Collectively, our findings demonstrated that Atu1027 functions as an aerotaxis receptor that affects agrobacterial chemotaxis and the invasion of *A. tumefaciens* into its host.

1 **An Aerotaxis Receptor Influences Invasion of *Agrobacterium***

2 ***tumefaciens* into Its Host**

3 Zhiwei Huang[1*], Junnan Zou[1], Minliang Guo[2], Guoliang Zhang[1], Jun Gao[1],

4 Hongliang Zhao[1], Feiyu Yan[1], Yuan Niu[1], Guang-Long Wang[1]

6 [1] *Jiangsu Provincial Agricultural Green and Low Carbon Production Technology Engineering*

7 *Research Center, School of Life Science and Food Engineering, Huaiyin Institute of Technology,*

8 *Huai'an, 223003, China*

9 [2] *College of Bioscience and Biotechnology, Yangzhou University, Yangzhou, 225009, China*

11 *Please address all correspondence to: Zhiwei Huang

12 (huangzhiwei@hyit.edu.cn)

13 ------------

14 Dr. Zhiwei Huang

15 School of Life Science and Food Engineering,

16 Huaiyin Institute of Technology,

17 Huai'an, 223003, China

18 Tel: 0517-83559216

19 E-mail: huangzhiwei@hyit.edu.cn

20 **Short title: Aerotaxis Receptor Influences Invasion**

Abstract

24 *Agrobacterium tumefaciens* is a soil-borne pathogenic bacterium that causes crown

25 gall disease in many plants. Chemotaxis offers *A. tumefaciens* the ability to find its

26 host and establish infection. Being an aerobic bacterium, *A. tumefaciens* possesses

27 one chemotaxis system with multiple potential chemoreceptors. Chemoreceptors

28 play an important role in perceiving and responding to environmental signals.

29 However, the studies of chemoreceptors in *A. tumefaciens* remain relatively

30 restricted. Here, we characterized a cytoplasmic chemoreceptor of *A. tumefaciens*

31 C58 that contains an N-terminal globin domain. The chemoreceptor was

32 designated as Atu1027. The deletion of Atu1027 not only eliminated the aerotactic

33 response of *A. tumefaciens* to atmospheric air but also resulted in a weakened

34 chemotactic response to multiple carbon sources. Subsequent site-directed

35 mutagenesis and phenotypic analysis showed that the conserved residue His100 in

36 Atu1027 is essential for the globin domain's function in both chemotaxis and

37 aerotaxis. Furthermore, deleting Atu1027 impaired the biofilm formation and

38 pathogenicity of *A. tumefaciens*. Collectively, our findings demonstrated that

39 Atu1027 functions as an aerotaxis receptor that affects agrobacterial chemotaxis

40 and the invasion of *A. tumefaciens* into its host.

42 **Keywords** *Agrobacterium tumefaciens*, chemotaxis, aerotaxis, chemoreceptor,

43 biofilm formation, pathogenicity

Introduction

46 *Agrobacterium tumefaciens* (reclassified as *Agrobacterium fabrum*) is a soil-

47 borne phytopathogen that causes crown gall disease in a wide range of

48 dicotyledonous plants and some gymnosperms (*Gelvin, 2012*; *Păcurar et al., 2011*).

49 It can transfer its T-DNA (transferred DNA) into the host plant's genome, and

50 genetically transform the hosts (*Gelvin et al., 2017*; *Guo et al. 2019*). The

51 extraordinary capacity of horizontal gene transfer has made *A. tumefaciens* a

52 powerful and widely used tool for obtaining transgenic or gene-edited plants (*Guo*

53 *et al., 2019*; *Huang et al., 2018*). *A. tumefaciens* is also a model microorganism to

54 study the interaction between microbes and plant hosts, or microbes (*Brown et al.,*

55 *2023*; *Lang & Faure, 2014*). *A. tumefaciens* usually distributes around the plant

56 rhizosphere. They specifically sense and recognize some signal molecules, such as

57 phenolic compounds (acetosyringone, hydroxy-acetosyringone) and sugar

58 compounds, released by wounded plant tissue (*Păcurar et al., 2011*). Chemotaxis

59 offers *A. tumefaciens* cells the ability to track these environmental cues and move

60 toward the plants, which is crucial for *A. tumefaciens* to find and infect host plants.

61 In the last four decades, the molecular mechanism of the pathogenicity of *A.*

62 *tumefaciens* and horizontal gene transfer from *A. tumefaciens* to host plants has

63 been well understood (reviewed in *Bourras, Rouxel & Meyer, 2015*; *Gelvin et al.,*

64 *2017*; *Guo et al. 2019*; *Matveeva & Lutova, 2014*). At the same time, research on

65 the molecular mechanism of *A. tumefaciens* chemotaxis has lagged.

66   As a typical behavior of bacteria, chemotaxis has been well-studied in

67   *Escherichia coli* (*Bi & Sourjik, 2018*; *Flack & Parkinson, 2022*; *Parkinson,*

68   *Hazelbauer & Falke, 2015*). The chemotaxis system of *E. coli* contains five

69   chemoreceptors and six core components: CheA, CheW, CheY, CheB, CheR, and

70   CheZ. Two chemoreceptor trimers of dimers, a histidine autokinase CheA dimer,

71   and two coupling proteins CheW form a ternary signaling complex at the cell poles

72   (*Parkinson, Hazelbauer & Falke, 2015*). In the ternary signaling complex,

73   chemoreceptors perceive and bind to diverse signal molecules through the

74   utilization of their ligand-binding domains (LBDs) (*Bi & Sourjik, 2018*). CheW

75   couples the autophosphorylation activity of CheA to chemoreceptor control (*Flack*

76   *& Parkinson, 2022*). The phosphorylated CheA transfers its phosphoryl groups to

77   the response regulator protein CheY and the methylesterase CheB. The

78   phosphorylated CheY is accountable for eliciting alterations in the flagellar

79   rotation direction, transitioning from counterclockwise (CCW) to clockwise (CW)

80   (*Huang et al., 2018*). On the other hand, the phosphorylated CheB, in collaboration

81   with the methyltransferase CheR, is employed to fine-tune the chemoreceptors'

82   sensitivity to external stimuli (*Parkinson, Hazelbauer & Falke, 2015; Salah Ud-*

83   *Din & Roujeinikova, 2017*). Upon binding to chemoattractants, the ternary signal

84   complex undergoes conformational changes, leading to the inhibition of

85   autophosphorylation of CheA. This inhibition results in a decrease in the flow of

86   CheA phosphoryl groups to CheY and CheB. The phosphorylated form of CheY is

87   also susceptible to dephosphorylation by its associated phosphatase CheZ

88   (*Parkinson, Hazelbauer & Falke, 2015*). Consequently, the short half-life of

89   phosphorylated CheY enables the bacterial cells to respond to chemotactic stimuli

90   in a unidirectional manner. Simultaneously, the reduction in phosphorylated CheB

91   allows CheR to continue methylating chemoreceptors. Methylation increases

92   chemoreceptors' ability to activate CheA, resulting in adaptation (*Parkinson,*

93   *Hazelbauer & Falke, 2015; Salah Ud-Din & Roujeinikova, 2017*).

94   In bacteria, chemoreceptors can recognize a variety of chemoeffectors.

95   Chemoeffectors encompass a range of chemical compounds or salts, such as sugars

96   (*Day et al., 2016*; *Ye et al., 2020*), amino acids (*Kumar Verma, Samal &*

97   *Chatterjee, 2018*; *Ye et al., 2020*), indole-3-acetic acid (*Rico‑Jiménez et al., 2022*),

98   and metal ions (*Shi et al., 2017*). Additionally, certain environmental factors, such

99   as light (*Perlova et al., 2022*), redox (*Xie et al., 2010*), pH (*Sweeney et al., 2012*),

100 and oxygen (*Bibikov et al., 1997*; *Garcia et al., 2017*). Oxygen plays a crucial role

101 in the survival of aerobic and microaerophilic microorganisms (*Zhulin et al., 1996*).

102 Aerotaxis, a process reliant on chemoreceptors to detect oxygen or redox

103 alterations, enables microorganisms to navigate towards areas with optimal oxygen

104 concentrations, facilitating various biological processes such as energy generation

105 and nitrogen fixation (*Jiang et al., 2016*; *Zhulin et al., 1996*). In the last three

106 decades, aerotaxis has attracted the attention of many researchers and several

107 oxygen-related chemoreceptors have been identified in bacteria and archaea

108 (*Arrebola & Cazorla, 2020*; *Bibikov et al., 1997*; *Freitas et al., 2005*; *Garcia et al.,*

109 *2017*; *Hou et al., 2000, 2001a, 2021b*; *Jiang et al., 2016*; *Tumewu et al., 2022*).

110   The ligand-sensing specificity of chemoreceptors is affected by the type of

111 LBDs. Two types of LBDs within chemoreceptors have been proven to be

112 involved in aerotaxis (*Edwards, Johnson & Taylor, 2006*; *Freitas et al., 2005*; *Hou*

113 *et al., 2000*; *Xie et al., 2010*). The first LBD, known as the Per-Arnt-Sim (PAS)

114 domain, serves a multifaceted role. Certain chemoreceptors that possess the PAS

115 domain function as redox sensors, monitoring alterations in the redox status of the

116 electron transport system through the flavin adenine dinucleotide (FAD) cofactor

117 associated with their PAS domains (*Edwards, Johnson & Taylor, 2006*; *Xie et al.,*

118 *2010*). This enables the cells to actively seek out favorable oxygen conditions. On

119 the other hand, other chemoreceptors employ their PAS domains to directly sense

120 oxygen through a heme-bound cofactor, thereby regulating aerotaxis (*Jiang et al.,*

121 *2016*; *Garcia et al., 2017*; *Tumewu et al., 2022*). The second LBD corresponds to

122 the globin domain, and chemoreceptors containing this domain serve as direct

123 oxygen sensors reliant on heme cofactor (*Freitas et al., 2005*; *Hou et al., 2000*). In

124 addition, it has been observed that certain chemoreceptors, characterized by

125 possessing 4-helix-bundle (4HB)-type LBDs, exhibit responsiveness to variations

126 in proton motive force in aerotaxis, exemplified by Tsr in *E. coli* (*Edwards,*

127 *Johnson & Taylor, 2006*). However, the specific involvement of 4HB-type LBDs

128 in aerotaxis remains uncertain. Moreover, aside from their involvement in

129 chemotaxis and aerotaxis , the identified oxygen-related chemoreceptors also play

130 a role in the interactions between microorganisms and their hosts (*Arrebola &*

131 *Cazorla, 2020*; *Garcia et al., 2017*; *Jiang et al., 2016*; *Tumewu et al., 2022*).

132 Consequently, investigating oxygen-related chemoreceptors will provide insights

133 into the physiological mechanisms of microorganisms and their interactions with

134 hosts.

135   *A. tumefaciens* strains possess numerous genes that are predicted to encode

136 chemoreceptors (*Shi et al., 2017*; *Wood et al., 2001*; *Xu et al., 2020*). Large

137 numbers of chemoreceptors in *A. tumefaciens* suggest that the bacteria can detect

138 diverse chemical molecules or environmental stimuli to navigate the way to

139 favorable ecological niches (*Xu et al., 2020*). To date, the identification of

140 chemoreceptors in *A. tumefaciens* has been limited to only four (*Shi et al., 2017*;

141 *Wang et al., 2021*; *Ye et al.,2020*; *Zong et al., 2022*). In the case of *A. tumefaciens*

142 C58, Atu0514, which is predicted to possess a globin domain as its LBD, has been

143 implicated in the chemotactic response to sucrose, valine, citric acid, and

144 acetosyringone (AS) (*Ye et al., 2020*). Atu0526 has been found to use a single-

145 Cache domain as LBD to bind the broad antibacterial agent formic acid (*Wang et*

146 *al., 2021*). Additionally, Atu1912, another chemoreceptor featuring a single-Cache

147 domain, has been shown to mediate the attractant response to pyruvate and the

148 repellent response to propionic acid. The ligands of single-Cache domain within

149 Atu1912 are pyruvate and propionic acid (*Zong et al., 2022*). In another strain, *A.*

150   *tumefaciens* GW4, a putative chemoreceptor harbors undefined LBD not only

151   regulated the chemotactic response towards trivalent arsenic, but also affected

152   trivalent arsenic oxidation, trivalent arsenic resistance, and bacterial growth (*Shi et*

153   *al., 2017*). However, chemoreceptors related to oxygen have not yet been identified

154   in *A. tumefaciens*.

155   In this study, we characterized a globin domain-containing chemoreceptor in

156   *A. tumefaciens* C58 named Atu1027 and showed that Atu1027 is a globin-coupled

157   sensor that modulates aerotaxis and chemotaxis. We also analyze the impact of

158   Atu1027 on biofilm formation and pathogenicity of *A. tumefaciens*.

159   **Materials & Methods**

160   *Bacterial strains, plasmids, media, and growth conditions*

161   All *Escherichia coli* and *Agrobacterium tumefaciens* strains and plasmids

162   used in this study are described in Table S1. *E. coli* strains were grown in the

163   lysogeny broth (LB) medium with or without 1.5 % agar at 37 °C or 25°C. *A.*

164   *tumefaciens* C58 and its derivatives were grown in MG/L medium or AB-sucrose

165   medium at 28 °C (*Cangelosi et al. 1991*; *Gelvin, 2006*). The final concentrations of

166   antibiotics: for *E. coli*, ampicillin (Ap) at 100 μg/ml, kanamycin (Km) at 50 μg/mL,

167   carbenicillin (Cr) at 25 μg/mL, tetracycline (Tc) at 15 μg/mL, chloramphenicol

168   (Cm) at 34 μg/ml; for *A. tumefaciens*, kanamycin (Km) at 100 μg/mL.

169   *DNA manipulations*

170   Molecular manipulations of DNA were conducted according to standard

171   molecular procedures. All primers used in this study are described in Table S2.

172   Purification of PCR products and DNA fragments from agarose gels was

173   performed by using FastPure Gel DNA Extraction Mini Kit (Vazyme Biotech,

174   Nanjing, China). Plasmid DNA was purified with the TIANprep Mini Plasmids Kit

175   (Tiangen Biotech, Beijing, China). According to the Inoue protocol, the competent

176   cells of *E. coli* were prepared (*Inoue, Nojima & Okayama*, 1990). The plasmid

177   DNA was transferred by heat shock into *E. coli* competent cells (*Sambrook et al.*

178   *1989*). The competent cells of *A. tumefaciens* were prepared as previously

179   described (*Cangelosi et al., 1991*). All plasmids were electrotransformed into *A.*

180   *tumefaciens* strains using an Eppendorf Eporator (Eppendorf AG, Hamburg,

181   Germany).

182   *Construction of deletion, complementation, or point mutants of A. tumefaciens*

183   Following the principle of homologous recombination, the precise deletion of

184   *the atu1027* gene in *A. tumefaciens* C58 was constructed by the procedures as

185   previously described (*Guo, Zhu & Gao D, 2009*). The gene-deletion strategy was

186   shown in Fig. S1. Briefly, a fusion of 585-bp upstream and 587-bp downstream of

187   the *atu1027* open reading frame (ORF) was inserted into the suicide plasmid

188   pEX18Km via the *Bam*H I and *Eco*R I restriction sites, resulting in the creation of

189   pEX-d1027. In pEX18Km and its derived plasmids, the kanamycin-resistant gene

190   *nptIII* was used as a positive selection marker, the suicide gene *sacB* was used as a

191   counterselection marker (*Huang et al., 2018*). Subsequently, pEX-d1027 was

192   introduced into *A. tumefaciens* C58. Two rounds of selection were conducted to

193   identify potential gene-deficient mutants. The colonies were further subjected to

194   PCR screening and DNA sequencing for verification purposes. The avirulent

195   mutant C58ΔvirA was constructed using the same strategy. The complemented

196   strain of the *atu1027*-deficient mutant was implemented by the introduction of the

197   plasmid pCB301-1027. The plasmid pCB301-1027 carries a 479-bp promoter

198   region and a 1500-bp intact ORF of the *atu1027* gene.

199   To substitute the conserved histidine residue at position 100 within the globin

200   region of Atu1027 with alanine, two single-residue mutation primers (cp1027-

201   H100A-2 and cp1027-H100A-3) were designed (Table S2). Two primers for

202   amplifying the *atu1027* expression cassette, in conjunction with the two single-

203   residue mutation primers, were utilized to procure two DNA fragments. The

204   specific site of the two base mutations is situated within the region of overlap

205   between the two aforementioned DNA fragments. Using overlap PCR, the *atu1027*

206   expression cassette containing the two base mutation sites was generated and

207   subsequently inserted into the plasmid pCB301 via the *Bam*H I and *Eco*R I

208   restriction sites. The recombinant plasmid pCB-1027H100A was then introduced

209   into the *atu1027*-deficient mutant via electroporation.

210   *Bacterial Two-Hybrid Assay*

211   The bacterial two-hybrid system (Stratagene, Agilent Technologies Inc., Santa

212   Clara, CA, USA) was used to detect potential protein–protein interactions. The

213 ORF of *atu1027* was amplified and inserted into the bait plasmid pBT to express

214 λcI-Atu1027 fusion protein. The ORFs of *cheW₁* and *cheW₂* were amplified and

215 inserted into the target plasmid pTRG to express CheW1–RNAP and CheW2–

216 RNAP fusion proteins, respectively. Then the recombinant target plasmid and bait

217 plasmid were collectively transferred into *E. coli* XL1-Blue MR competent cells by

218 heat shock and spread on LB-CTCK plates for screening positive clones. The LB-

219 CTCK medium is made up of LB medium, 25 μg/mL carbenicillin, 15 μg/mL

220 tetracycline, 34 μg/mL chloramphenicol, and 50 μg/mL kanamycin. The positive

221 clones in the LB-CTCK plates were picked out and streaked onto a new LB-TCK

222 plate that contains 15 μg/mL tetracycline, 34 μg/mL chloramphenicol, 50 μg/mL

223 kanamycin, 80 μg/mL X-gal, and 0.2 mM galactosidase inhibitor. The LB-TCK

224 plate with positive clones was placed in a lightless biochemical incubator at 37°C

225 for 16 h. The galactosidase activity of different groups was quantified as

226 previously described (*Ye et al., 2021*).

227 *Protein expression, pull-down assay and immunoblotting*

228   *E. coli* BL21 (DE3) was employed as the host organism for the

229 overproduction of Atu1027-His, Atu1027H100A-His, CheW1, CheW2, and SalT-

230 His. SalT-His, which is unrelated to chemotaxis, served as the negative control. *E.*

231 *coli* cells containing the respective recombined pET-30a plasmids were cultivated

232 until reaching a cell density of approximately 5×10^8 cell/mL. Subsequently,

233 isopropylthio-β-D-galactoside (IPTG) was added to the cultures at a final

234 concentration of 0.2 mM to induce the expression of the fusion proteins. After

235 being cultivated at 25 °C for 6 hours, the cells were centrifuged 5000 × g for 10

236 minutes, washed twice and resuspended in PBS buffer (10 mM, pH 7.4). The pull-

237 down assay was conducted in accordance with the methodology described in a

238 previous study (*Huang et al., 2018*). The cell suspension was subjected to

239 sonication until it reached a state of near clarity, and the supernatant from this

240 sonicated cell suspension was collected through centrifugation at a force of 12,000

241 × g for a duration of 30 minutes. Different supernatants were then respectively

242 introduced into 1mL Ni-IDA Resins (Sangon Biotech, Shanghai, China). The

243 fusion protein-bound resins were subjected to five washes with PBS buffer and

244 subsequently incubated with 2 mL of cell crude extract derived from a 50 mL cell

245 culture that overproduced either CheW1 or CheW2. Following a 1-hour incubation

246 at 4 °C with gentle shaking, the resins were washed with 10 volumes of PBS buffer

247 containing increasing concentrations of imidazole (10 mM, 30 mM, and 50 mM) to

248 remove nonspecifically bound proteins. The specifically bound proteins were then

249 eluted from the resins using 500 µL of PBS buffer containing 250 mM imidazole.

250 5 µL of eluent obtained from distinct samples were subjected to SDS-PAGE. For

251 immunoblotting, proteins were transferred onto hydrophilic polyvinylidene

252 difluoride membranes (Merck Millipore, Billerica, MA, USA) through

253 electrophoresis. The visualization of the transferred proteins was achieved using

254 the BCIP/NBT alkaline phosphatase color development kit (Beyotime

255 biotechnology, Shanghai, China), following the recommended protocol provided

256 by the manufacturer. To obtain antibodies capable of distinguishing between two

257 CheWs, peptide fragments corresponding to the variable sequences of CheW1

258 (amino acid residues 142-155) and CheW2 (amino acid residues 146-159) were

259 synthesized artificially and utilized as antigens for antibody generation in New

260 Zealand rabbits (*Huang et al., 2018*).

261 *Air trap assay for aerotaxis*

262 The procedure for the air trap assay was followed as described by Arrebola

263 (2020) with some modifications (*Arrebola and Cazorla, 2020*). To establish an air

264 trap, a modified Pasteur pipette was initially placed within a glass tube, covered

265 with a lid, and subjected to autoclaving. Next, sterile AB-sucrose medium

266 containing 0.1% agar was heated and carefully poured into the glass tube. The

267 liquid level of the medium was maintained 3 cm below the top of the Pasteur

268 pipette. Following this, 2 mL of paraffin oil was added to the glass tube but was

269 prevented from falling into the Pasteur pipette. Consequently, the paraffin oil acted

270 as a barrier, effectively isolating the external medium of the Pasteur pipette from

271 the surrounding air and creating a localized hypoxic environment. Only the

272 medium contained within the Pasteur pipette was able to interact with the air and

273 undergo air exchange. Subsequently, *A. tumefaciens* strains that grew to the

274 middle-logarithmic growth phase were gently centrifuged at $3500 \times g$ for 3

275 minutes and resuspended in fresh AB-sucrose medium to achieve an OD_{600nm} of 0.6.

276 100 µL of bacterial cells were slowly injected into AB-sucrose medium with a

277 disposable sterilized syringe but outside of the Pasteur pipette. The inoculation site

278 was positioned 2 cm above the base of the Pasteur pipette. If the bacteria possess

279 oxygen-sensing capabilities, they would exhibit movement towards the interior of

280 the Pasteur pipette. Finally, the air trap devices were placed in a biochemical

281 incubator without any disturbance and observed every 12 hours, until the bacterial

282 population was visible.

283 *Aerotaxis behavior observation*

284   The aerotaxis behavior observation was conducted as previously described

285 with some modifications (*Arrebola & Cazorla, 2020*). *A. tumefaciens* strains were

286 grown in AB-sucrose medium to middle-logarithmic growth phase, centrifuged at

287 $3500 \times g$ for 3 minutes, and suspended at the same cell density (1×10^8 cfu/mL) in

288 chemotaxis buffer (10 mmol/L KH_2PO_4, 0.1 mmol/L EDTA, pH 7.0) with 14.6

289 mM sucrose as the energy source. 3 µL drop of bacterial cells was deposited on a

290 coverslip, the coverslip was inverted on an excavated slide. As a result, the drop

291 was surrounded by air. The bacterial behavior was monitored by optical

292 microscopy at $1000 \times$ magnification. The photographs of bacterial behavior at the

293 edges of the droplets were taken after 5, 10, and 15 minutes. To prevent bacterial

294 motility from being orientated by the light during the photo interval, the

295 microscope light was turned off.

296 *Chemotaxis assays*

297   Chemotaxis to different oxidizable substrates in a spatial gradient was assayed

298   in the soft agar plates containing AB-medium, 0.2 % Bacto agar (Beyotime

299   Biotech, Shanghai, China), and 15 mM single carbon source. The carbon sources

300   included mannitol, xylose, fructose, sucrose, glucose, and galactose. *A.*

301   *tumefaciens* cells were grown and collected as indicated above for aerotaxis. The

302   tested cell cultures were normalized to an OD_{600nm} of 0.6. 3 μL of tested cell

303   suspension was inoculated into the soft agar plates and incubated for 36 h without

304   disturbance. The diameter of the colonies was measured and used to quantify the

305   chemotaxis to different carbon sources.

306   *Biofilm formation assays*

307   *A. tumefaciens* cells in the middle-logarithmic growth phase were collected

308   and normalized to an OD_{600} of 0.1. 2 mL of culture was added to a sterile glass

309   tube. The tubes were incubated for 72 h. For crystal violet (CV) visualization, the

310   tube was washed thoroughly with double-distilled H_2O and stained with 0.15 %

311   (wt/vol) crystal violet staining solution for 15 minutes. After the staining procedure,

312   the tubes were washed five times with double-distilled H_2O to remove the crystal

313   violet staining solution. The formation of purple ring-like structures on the tube

314   was observed. Finally, the crystal violet is eluted off with 30% acetic acid (vol/vol).

315   The eluent is measured at 570 nm to determine the strength of biofilm formation. A

316   normalization of absorbance values to culture growth was achieved by dividing the

317   solubilized CV OD_{570} value by the planktonic cell OD_{600} value. All strains were

318 performed in three replicates.

319 *Tumorigenesis assays*

320   The tumorigenesis assays on the leaves of the *Kalanchoe* plant were

321 implemented as described previously with some modifications (*Yang et al., 2020*).

322 Different *A. tumefaciens* strains were prepared as in the air trap assay described

323 previously. An avirulent strain C58ΔvirA was used as a negative control. The

324 agrobacterial cells were resuspended in AB-sucrose liquid medium at 5×10^8

325 cfu/mL for inoculation. *Kalanchoe* plants' leaves that grew for more than three

326 weeks were selected for the infection. Before inoculation, several wound lines

327 were made in the *Kalanchoe* leaf by using a sterile scalpel. Each wound line was

328 inoculated with 3 μL of different cell suspensions. The infected *Kalanchoe* plants

329 were grown in the pots at room temperature for 30-40 days. The tumours in the

330 wound lines were photographed and weighed. Each inoculation was repeated at

331 least three times on separate leaves.

332 *Statistical analysis*

333 The data were presented as the mean ± standard error of three replicates using

334 analysis of variance (ANOVA). To assess the significance of differences between

335 various groups, the Student-Newman-Keuls (SNK) multiple comparison test was

336 employed at a significance level of $P < 0.05$.

337 **Results**

338 *Atu1027 is a cytoplasmic chemoreceptor containing a globin domain*

339   The globin domain of the heme-containing transducers (HemAT-Bs from

340   *Bacillus subtilis* and HemAT-Hs from *Halobacterium salinarum*) can bind

341   diatomic oxygen and mediate aerotactic reactions in bacteria and archaea (*Hou et*

342   *al., 2000*; *2021a*). *A. tumefaciens* C58 has 20 genes coding putative

343   chemoreceptors on its genome (*Wood et al., 2001*). Among these genes, *atu1027*,

344   which is located on the circular chromosome, is predicted to encode a

345   chemoreceptor (accession number: WP_010971342.1) with a globin domain

346   (Figure 1A). The analysis conducted using Pfam revealed that the peptide chain of

347   the globin domain within Atu1027 encompasses 159 amino acid residues. A prior

348   investigation proposed that the globin domains of Atu1027, HemAT-Bs, and

349   HemAT-Hs evolved from a shared ancestral globin (*Freitas et al., 2005*). In the

350   present study, amino acid sequence alignment (Figure 1B) indicated that the globin

351   domain of Atu1027 shares 17.65% sequence identity with that of HemAT-Bs and

352   18.64% sequence identity with that of HemAT-Hs. The alignment of the sequence

353   also demonstrated that the globin domain of Atu1027 retains two strictly conserved

354   residues present in all globin domains (*Hou et al., 2021a*). The analysis conducted

355   using the DeepTMHMM (https://dtu.biolib.com/DeepTMHMM) and ProtScale

356   (https://web.expasy.org/protscale/) online tools indicated that Atu1027 does not

357   possess a transmembrane domain. Furthermore, the sequence of amino acids in

358   Atu1027 is highly conserved among *Agrobacterium* species (Fig. S2). These

359   findings suggested that Atu1027 potentially functions as a cytoplasmic

360 chemoreceptor involved in mediating aerotaxis in *Agrobacterium species*.

361 *Atu1027 interacts with CheW1 and CheW2*

362  In the chemotaxis system of *E. coli*, the formation of the ternary signaling

363 complex relies on the interaction of chemoreceptors and the unique coupling

364 protein CheW (*Parkinson, Hazelbauer & Falke, 2015*). *A. tumefaciens* C58 two

365 coupling proteins, namely CheW1 and CheW2 (*Huang et al., 2018*; *Wood et al.,*

366 *2001*). In light of the hypothesis that Atu1027 serves as a cytoplasmic

367 chemoreceptor, it is crucial to validate the potential interaction between Atu1027

368 and two CheWs. To assess the protein-protein interactions, the bacterial two-

369 hybrid and *in vitro* His-tag pull-down assays were employed. In the bacterial two-

370 hybrid assay, the presence of blue colonies on the designated plates serves as an

371 indication of the interaction between the target protein and the bait protein. The

372 intensity of the blue color corresponds to the strength of the protein-protein

373 interaction and the level of ß-galactosidase activity. As illustrated in Figure 2A and

374 2B, the experimental groups (CheW1+Atu1027 and CheW2+Atu1027) displayed a

375 higher β-galactosidase activity compared to the negative control group. In the His-

376 tag pull down assay (Figure 2C), both CheW1 and CheW2 were identified in the

377 eluate from the resin bound with Atu1027-His, while they were absent in the

378 negative control (the resin bound with SalT-His). This outcome serves as

379 confirmation that both CheW1 and CheW2 can interact with Atu1027 in an *in vitro*

380 setting. Consequently, the results indicated that Atu1027 interacts with either

381 CheW1 or CheW2.

382 *Atu1027 is an aerotaxis receptor in A. tumefaciens C58*

383 In order to ascertain the functions of Atu1027, a precise deletion of *atu1027*

384 in *A. tumefaciens* C58 was accomplished via homologous recombination, as

385 outlined in the Materials and Methods section. The resulting *atu1027*-deficient

386 mutant was denoted as C58Δ1027. Subsequently, the *atu1027* gene, along with its

387 native promoter (located 479 bp upstream of *atu1027*), was reintroduced into the

388 C58Δ1027 mutant using a plasmid, thereby restoring the expression of Atu1027

389 protein in C58Δ1027. This complemented strain was designated as C58Δ1027+.

390 The bioinformatic analysis and protein interaction experiments provided

391 indications that Atu1027 could potentially function as an aerotaxis receptor in *A.*

392 *tumefaciens*. In order to validate this hypothesis, the aerotaxis of various *A.*

393 *tumefaciens* strains was assessed using air trap assays and optical microscope

394 observations.

395 The results of the air trap assays are presented in Figure 3. At 72 h post-

396 inoculation, the device containing the complemented strain C58Δ1027+ exhibited a

397 significant aggregation of bacterial cells on the surface of the semi-solid medium

398 in the Pasteur pipette. In contrast, no such phenomenon was observed in the device

399 containing the wild-type C58 or the *atu1027*-deficient mutant C58Δ1027. At 96 h

400 post-inoculation, the wild-type C58 cells displayed visible aggregation on the

401 surface of the semi-solid medium, while the medium inoculated with C58Δ1027

402   remained clear in the Pasteur pipette. At 120 h post-inoculation, the medium

403   inoculated with C58Δ1027 remained clear on the surface of the medium in the

404   Pasteur pipette. The results above indicated that the deletion of *atu1027* eliminates

405   the aerotactic response of *A. tumefaciens* to atmospheric air. Furthermore, we

406   conducted growth curve experiments in AB-sucrose liquid medium to determine if

407   the deletion of *atu1027* affects the growth rate of *A. tumefaciens*. The growth rates

408   of C58Δ1027 and C58Δ1027+ were comparable to that of the wild-type C58 (Fig.

409   S4), and the difference was not statistically significant (P value > 0.05). Hence, the

410   deletion of *atu1027* did not affect the normal growth of *A. tumefaciens*.

411   Subsequently, an optical microscope was employed to perform continuous

412   monitoring of the aerotaxis exhibited by the tested agrobacterial strains. The

413   bacterial cells were deposited onto a coverslip, which was promptly inverted onto

414   an excavated slide. To prevent air infiltration, Vaseline was applied to all four

415   sides of the coverslip. The slide was then positioned on the objective table of the

416   optical microscope and observed at 5-minute intervals. The findings are illustrated

417   in Figure 4. At 5 minutes post-inoculation, C58 and C58△1027+ cells began to

418   accumulate at the boundary of bacterial suspension and air. The quantity of C58

419   and C58△1027+ cells was significantly higher compared to that of C58△1027. At

420   10 and 15 minutes post-inoculation, there was further accumulation of C58 and

421   C58△1027+ cells at the boundary between the bacterial suspension and the air,

422 while the number of C58△1027 cells did not show a significant increase. These

423 results are consistent with the results obtained from the air trap assays. Collectively,

424 it can be concluded that Atu1027 is an aerotaxis receptor that modulates in the

425 aerotaxis of *A. tumefaciens* under the test condition.

426 *Atu1027 is involved in the chemotaxis of A. tumefaciens*

427   In *A. tumefaciens* C58, CheW1 and CheW2 are involved in the formation of

428 ternary signaling complexes at the cell poles (*Huang et al., 2018*). Atu1027

429 interacts with both CheW1 and CheW2, indicating its role as a component of the

430 chemotaxis system in *A. tumefaciens*. The deletion of the *atu1027* gene may have

431 an impact on the chemotactic abilities of *A. tumefaciens*. Therefore, in order to

432 assess the chemotaxis of *A. tumefaciens*, six common carbon sources (mannitol,

433 xylose, fructose, sucrose, glucose, galactose) were tested on the swim agar plates.

434 As shown in Figure 5, in six different kinds of semi-solid AB-medium containing

435 different sugars, the swimming halo of the *atu1027*-deficient mutant C58Δ1027 is

436 slightly smaller than that of wild-type C58, demonstrating that the deletion of

437 *atu1027* slightly reduced the chemotactic response to multiple carbon sources in *A.*

438 *tumefaciens*. Additionally, when the *atu1027* gene was re-introduced into the

439 *atu1027*-deficient mutant C58Δ1027, the swimming halo of the complemented

440 strain C58Δ1027+ was bigger than that of wild-type C58. This may be caused by

441 an increased copy number of the *atu1027* gene in the complemental strain

442 C58Δ1027+.

443 *The replacement of His100 with alanine completely abolished the function of* the

444 globin domain of *Atu1027*

445   In the globin domains of HemAT-Bs and HemAT, the proximal histidine

446 residue (His-123) plays a crucial role in both oxygen sensing and heme binding

447 (*Freitas et al., 2005*; *Hou et al., 2000, 2021a*). Replacing the His-123 with alanine

448 eliminates the function of the globin domains (*Hou et al., 2001a*). The globin

449 domain of Atu1027 contains a histidine residue at position 100 (His100), which

450 has been predicted to serve as the heme binding site (Figure 1). Mutation on

451 His100 may also affect the function of Atu1027. Therefore, to assess the

452 importance of His100 for the function of Atu1027, a site-directed mutagenesis

453 technique was employed to replace His100 with an alanine residue. The H100A

454 mutant of Atu1027 was expressed in the C58Δ1027 strain, resulting in the creation

455 of the mutant strain C58Δ1027H100A. Chemotaxis assay and air trap assay for

456 aerotaxis were conducted to test the phenotype of the mutant strain

457 C58Δ1027H100A. As anticipated, the C58Δ1027H100A strain exhibited a

458 compromised chemotactic response to sucrose (Figure 6A and 6B) and did not

459 accumulate in the Pasteur pipette after 120 hours of inoculation (Figure 6C). These

460 phenotypic characteristics of C58Δ1027H100A were consistent with those of the

461 parental strain C58Δ1027. At the same time, mutation in His100 did not affect the

462 interactions between Atu1027 and two CheWs (Fig. S5). These results indicated

463 that His100 plays a crucial role in the functionality of the globin domain within

464   Atu1027. Additionally, this finding also provides evidence to support the point that

465   Atu1027 acts as an aerotaxis receptor.

466   *Deletion of atu1027 impaired the biofilm formation of A. tumefaciens in static*

467   *culture*

468   Biofilm formation is an integral aspect of the interactions between plants and

469   microbes, playing a critical role in the establishment of infections (*Bogino et al.,*

470   *2013*; *Danhorn & Fuqua, 2007*). In the soilborne pathogen *Ralstonia*

471   *solanacearum*, the normal formation of biofilms necessitates the involvement of

472   aerotaxis (*Yao et al., 2007*). Atu1027 serves as an aerotaxis receptor to modulate

473   chemotaxis in *A. tumefaciens*, the deletion of *atu1027* may impair the biofilm

474   formation of *A. tumefaciens*. Hence, the biofilm formation assays of *atu1027*

475   mutants were performed in static culture. As shown in Figure 7, at 72 h post-

476   inoculation, all strains under examination possess the ability to generate biofilms.

477   However, it is noteworthy that the biofilms produced by strains C58 and

478   C58Δ1027+ exhibit considerably greater strength compared to those formed by

479   C58Δ1027. This observation serves to validate the notion that the absence of

480   Atu1027 diminished the biofilm formation capacity of *A. tumefaciens* in static

481   culture.

482   *atu1027 is required for the full pathogenicity of A. tumefaciens*

483   The deletion of the *atu1027* gene impairs not only chemotaxis and aerotaxis

484   of *A. tumefaciens* but also its ability to form biofilm in static culture. Nevertheless,

485   it remains unknown the impact of deletion of *atu1027* on the pathogenicity of *A.*

486   *tumefaciens*. To investigate the potential effect of *atu1027* deficiency on the

487   pathogenicity of *A. tumefaciens*, three different strains were used: the wild type

488   C58, the *atu1027*-deficient mutant C58Δ1027, and the complemented strain

489   C58Δ1027+. These strains were individually inoculated onto the leaves of

490   *Kalanchoe* plants. All tested strains were precultured in AB-sucrose liquid medium

491   to mid-log phase, normalized to the same cell density, and inoculated on the

492   *Kalanchoe* plants' leaves. Based on the tumour photograph presented in Figure 8A,

493   it can be observed that, except the avirulent strain C58ΔvirA, other three tested

494   strains were capable of inducing tumours on the wound sites of *Kalanchoe* leaves

495   after 30 days of inoculation. However, the tumour induced by the C58Δ1027 was

496   smaller compared to those induced by the C58 and C58Δ1027+. The data

497   presented in Figure 8B further supports this observation, as it demonstrated that the

498   tumour weight induced by the strain lacking *atu1027* was significantly lower than

499   that induced by the other tested strains. Hence, it can thus be concluded that

500   deletion of *atu1027* gene attenuates the pathogenicity of *A. tumefaciens*.

501   **Discussion**

502   In the present study, we conducted a characterization of a cytoplasmic

503   chemoreceptor, Atu1027, in *A. tumefaciens* C58. Atu1027 was found to possess a

504   globin domain and functioned as both an aerotaxis receptor and a participant in the

505   chemotactic response to six oxidizable substrates. The globin domain was

506 identified as the heme-binding domain within globin-coupled sensors (GCS) (*Hou*

507 *et al., 2001a*). The GCS proteins are a group of putative O_2 sensors that contain an

508 N-terminal sensor domain, a variable middle domain, and a C-terminal output

509 domain (*Rivera et al., 2018*; *Walker et al., 2017*). Oxygen-dependent physiology

510 and phenotypes in microorganisms are likely controlled by GCS proteins. Based on

511 the C-terminal output domains, the GCS proteins can be categorized into various

512 types, including MCP, kinase, diguanylate cyclase (DGC), and adenylate cyclase

513 (AC) (*Walker et al., 2017*). Previous research has identified MCP-type GCS

514 proteins in the archaeon *H. salinarium* (*Hou et al., 2000*), as well as in two gram-

515 positive bacteria, *B. subtilis* and *Bacillus halodurans* (*Hou et al., 2000, 2001b*).

516 Our study provided evidence that Atu1027 functions as a typical MCP-type GCS

517 protein and serves as an aerotaxis receptor in the gram-negative bacteria *A.*

518 *tumefaciens*. The heme-binding site (His100) located within the globin domain of

519 Atu1027 plays a critical role in facilitating the chemotaxis and aerotaxis functions

520 of Atu1027. More importantly, the amino acid sequence of Atu1027 is highly

521 conserved among the chemoreceptors in different *Agrobacterium* species (Fig. S2).

522 This observation suggests that MCP-type GCS proteins are widely present in

523 *Agrobacterium*, potentially serving as the main aerotaxis receptor to facilitate

524 multiple physiological activities.

525   Moreover, it should be noted that Atu1027 is not the sole predicted

526 chemoreceptor that possesses a globin domain. The *atu0514* gene, located within

527 the chemotaxis operon of *A. tumefaciens* C58, also encodes a chemoreceptor that

528 contains a globin domain (*Xu et al., 2020*). Atu0514 affected the chemotactic

529 response of *A. tumefaciens* to various chemoeffectors, but its function in aerotaxis

530 has not been addressed (*Ye et al., 2021*). To further investigate, we conducted an

531 alignment of the globin domain of Atu0514 with that of HemAT-Bs, HemAT-Hs,

532 and Atu1027. Fig. S6 illustrated that three conserved amino acids, which are

533 present in all globins, were not identified within the globin domain of Atu0514.

534 Therefore, it is hypothesized that Atu0514 may possess unique characteristics that

535 distinguish it from typical globin domain-type chemoreceptors. Given its exclusive

536 presence as the sole chemoreceptor encoded by the chemotaxis operon of *A.*

537 *tumefaciens*, Atu0514 likely plays a crucial role in the transduction of chemotaxis

538 signaling.

539   In addition to the globin domain, the PAS domain is another common sensor

540 mediating aerotaxis occurring in chemoreceptors. However, the specific functions

541 of the PAS domain in chemoreceptors exhibit variability. The involvement of the

542 PAS domain in aerotaxis primarily encompasses two types of mechanisms. Type I

543 involves the binding of a redox-sensitive flavin adenine dinucleotide (FAD)

544 cofactor by the PAS domain to monitor changes in the redox status of the electron

545 transport system. Examples of this type include Aer in *E.coli* (*Bibikov et al., 2000*;

546 *Maschmann et al., 2022*) and AerC in *Azospirillum brasilense* (Xie et al., 2010).

547 The second mechanism, known as Type II, involves the PAS-containing

chemoreceptor binding to a heme cofactor. This binding enables the chemoreceptor

to sense oxygen and regulate aerotaxis, two typical examples of Type II

mechanism are IcpB in *Azorhizobium caulinodans* (Jiang et al., 2016) and Aer2 in

Pseudomonas aeruginosa (*Garcia et al., 2017*). Interestingly, type II is comparable

to that observed in the *B. subtilis*, but the heme cofactor was bonded by a globin-

coupled domain rather than a PAS domain (*Hou et al., 2000*). In the case of *A.*

tumefaciens, four putative chemoreceptors contain two PAS domains within their

N-terminal region, yet the precise function of these chemoreceptors remains

unknown (*Xu et al., 2021*). Based on our study findings, we propose that Atu1027

serves as an aerotaxis receptor. Both qualitative assays used in this study showed

that Atu1027 deletion prevents aerotaxis.

It is reported that chemotaxis and aerotaxis are required for normal biofilm

formation and interaction with the hosts (*Arrebola & Cazorla,2020*; *Greer-Phillips*

et al., 2004; *Hölscher et al., 2016*; *Ichinose et al., 2023*; *Jiang et al., 2016*;

Tumewu et al., 2022; *Yao et al., 2007*). Similar findings were observed in the

investigation of Atu1027, where the removal of *atu1027* resulted in a modest

reduction in biofilm formation and pathogenicity of *A. tumefaciens*. One potential

explanation for the disparity observed in biofilm formation between the *atu1027*-

deficient mutant and the wild-type C58 is the impaired capacity of *atu1027*-

deficient agrobacterial cells in response to the air, resulting in a reduced population

of bacterial cells at the liquid-air interface (Figure 4). This scarcity of bacterial

569 cells in close proximity to the solid-liquid interface could potentially hinder the

570 initial growth of the biofilm. Within further growth and maturation of the biofilm,

571 the local environment within the biofilm undergoes several changes, notably a

572 decrease in the availability of oxygen (*Stewart & Franklin, 2008*). Wild-type C58

573 with aerotaxis is more competitive when compared with C58Δ1027 without

574 aerotaxis. For the pathogenicity, when *A. tumefaciens* infects plants and forms

575 crown gall tumors on the wound sites, the oxygen concentration in the crown gall

576 tumors is also lower than that on the outside (*Gohlke & Deeken, 2014*). Wild-type

577 C58 carrying Atu1027 has an advantage in finding the appropriate oxygen

578 concentration over the *atu1027*-deficient mutant. An adequate oxygen supply is

579 more conducive to active physiological activity and promotes the enhancement of

580 the pathogenicity of *A. tumefaciens*. More importantly, compared with the biofilm

581 formed by C58Δ1027, the stronger biofilm formed by wild-type C58 also helps the

582 bacteria to establish a more effective infection and against harsh environmental

583 factors.

584 However, to our knowledge, the involvement of aerotaxis receptors in the

585 process of biofilm formation is controversial. Some of the aerotaxis receptors act

586 as a negative regulator in biofilm formation (*Jiang et al., 2016*; *Yao & Allen, 2007*),

587 while others serve as positive regulators (*Arrebola & Cazorla, 2020*; *Hölscher et*

588 *al., 2015*; *Tumewu et al., 2022*). Our results were in according with the latter. To

589 the best of our knowledge, there is still no literature that completely explains how

590 the aerotaxis receptor affects biofilm formation in microorganisms. In our opinion,

591 subsequent in-depth studies need to be done to explain the molecular mechanisms

592 of aerotaxis receptors in regulating biofilm formation. The investigation of cross-

593 talk between the chemotaxis signal transduction pathway and the biofilm formation

594 represents a promising avenue for further research. A recent study has found that

595 some chemoreceptors in *Comamonas testosteroni* CNB-1 can physically bind with

596 the components in the pathway of biofilm formation (*Huang et al., 2019*).

597 Additionally, the histidine kinase CheA has been observed to phosphorylate FlmD,

598 a response regulator that plays a crucial role in mediating biofilm formation

599 (*Huang et al., 2019*). Furthermore, the role of microbial species and their energy

600 metabolism types cannot be ignored.

601 **Conclusions**

602 Atu1027, a cytoplasmic chemoreceptor found in *A. tumefaciens* C58, exhibits an

603 N-terminal globin domain and serves as an aerotaxis receptor, governing the

604 organism's response to atmospheric air as well as its chemotactic movement

605 towards diverse oxidizable substrates. The conserved residue His100 within

606 Atu1027 plays a pivotal role in facilitating its globin domain's functionality in both

607 aerotaxis and chemotaxis. Furthermore, Atu1027 exerts influence over

608 agrobacterial chemotaxis and the invasion of *A. tumefaciens* into its host.

609

610 **Acknowledgments**

611 We thank Qingxuan Zhou (College of Bioscience and Biotechnology, Yangzhou

612 University) for the mutant construction. We thank Prof. Xiangqian Li, Dr. Shiyan

613 Wang, and Dr. Guodong Chen (School of Life Science and Food Engineering,

614 Huaiyin Institute of Technology) for their support in providing experimental

615 equipment.

616

617 **References**

618 **Arrebola E, Cazorla FM. 2020.** Aer receptors influence the *Pseudomonas chlororaphis* PCL1606 lifestyle.

619   *Frontiers in Microbiology* **11**:1560 DOI 10.3389/fmicb.2020.01560.

620 **Bashford D, Chothia C, Lesk A M. 1987.** Determinants of a protein fold: Unique features of the globin

621   amino acid sequences. *Journal of molecular biology* **196**(1):199-216 DOI 10.1016/0022-

622   2836(87)90521-3.

623 **Bi S, Sourjik V. 2018.** Stimulus sensing and signal processing in bacterial chemotaxis. *Current Opinion in*

624   *Microbiology* **45**:22-29 DOI 10.1016/j.mib.2018.02.002.

625 **Bibikov SI, Barnes LA, Gitin Y, Parkinson JS. 2000.** Domain organization and flavin adenine dinucleotide-

626   binding determinants in the aerotaxis signal transducer Aer of *Escherichia coli*. *Proceedings of the*

627   *National Academy of Sciences of the United States of America* **97**(11):5830-5835 DOI

628   10.1073/pnas.100118697.

629 **Bibikov SI, Biran R, Rudd KE, Parkinson JS. 1997.** A signal transducer for aerotaxis in *Escherichia coli*.

630   *Journal of Bacteriology* **179**(12):4075-4079 DOI 10.1128/jb.179.12.4075-4079.1997.

631 **Bogino P, Oliva M, Sorroche F, Giordano W. 2013.** The role of bacterial biofilms and surface components

632   in plant-bacterial associations. *International Journal of Molecular Sciences* **14**(8):15838-15859 DOI

633   10.3390/ijms140815838.

634 **Bourras S, Rouxel T, Meyer M. 2015.** *Agrobacterium tumefaciens* gene transfer: How a plant pathogen

635   hacks the nuclei of plant and nonplant organisms. *Phytopathology* **105**(10):1288-1301 DOI

636   10.1094/PHYTO-12-14-0380-RVW.

637   **Brown PJB, Chang JH, Fuqua C, Becker A. 2023.** *Agrobacterium tumefaciens*: a transformative agent for

638   fundamental insights into host-microbe interactions, genome biology, chemical signaling, and cell

639   biology. *Journal of Bacteriology* **205**(4):e00005-23 DOI 10.1128/jb.00005-23.

640   **Cangelosi GA, Best EA, Martinetti G, Nester EW. 1991.** Genetic analysis of *Agrobacterium*. *Methods in*

641   *Enzymology* **204**:384-397 DOI 10.1016/0076-6879(91)04020-O.

642   **Danhorn T, Fuqua C. 2007.** Biofilm formation by plant-associated bacteria. *Annual Review of Microbiology*

643   **61**:401-422 DOI 10.1146/annurev.micro.61.080706.093316.

644   **Day CJ, King RM, Shewell LK, Tram G, Najnin T, Hartley-Tassell LE, Wilson JC, Fleetwood AD,**

645   **Zhulin IB, Korolik V. 2016.** A direct-sensing galactose chemoreceptor recently evolved in invasive

646   strains of *Campylobacter jejuni*. *Nature communications* **7**(1):13206 DOI 10.1038/ncomms13206.

647   **Edwards JC, Johnson MS, Taylor BL. 2006.** Differentiation between electron transport sensing and proton

648   motive force sensing by the Aer and Tsr receptors for aerotaxis. *Molecular Microbiology* **62**(3):823-

649   837 DOI 10.1111/j.1365-2958.2006.05411.x.

650   **Flack CE, Parkinson JS. 2022.** Structural signatures of *Escherichia coli* chemoreceptor signaling states

651   revealed by cellular crosslinking. *Proceedings of the National Academy of Sciences of the United*

652   *States of America* **119**(28) DOI 10.1073/pnas.2204161119.

653   **Freitas TA, Saito JA, Hou S, Alam M. 2005.** Globin-coupled sensors, protoglobins, and the last universal

654   common ancestor. *Journal of inorganic biochemistry* **99**(1):23-33. 10.1016/j.jinorgbio.2004.10.024.

655   **Garcia D, Orillard E, Johnson MS, Watts KJ. 2017.** Gas Sensing and Signaling in the PAS-Heme Domain

656   of the *Pseudomonas aeruginosa* Aer2 Receptor. *Journal of Bacteriology* **199**(18): e00003-17 DOI

657   10.1128/JB.00003-17.

658   **Gelvin SB. 2006.** *Agrobacterium* virulence gene induction. *Methods in molecular biology* **343**:77-84 DOI

659   10.1385/1-59745-130-4:77.

660   **Gelvin SB. 2012.** Traversing the cell: *Agrobacterium* T-DNA's journey to the host genome. *Frontiers in Plant*

661   *Science* **3**:52 DOI 10.3389/fpls.2012.00052.

662   **Gelvin SB. 2017.** Integration of *Agrobacterium* T-DNA into the plant genome. *Annual Review of Genetics*

663   **51**:195-217 DOI 10.1146/annurev-genet-120215-035320.

664 **Gohlke J, Deeken R. 2014.** Plant responses to *Agrobacterium tumefaciens* and crown gall development.

665   *Frontiers in Plant Science* **5**:155 DOI 10.3389/fpls.2014.00155.

666 **Greer-Phillips SE, Alexandre G, Taylor BL, Zhulin IB. 2003.** Aer and Tsr guide *Escherichia coli* in spatial

667   gradients of oxidizable substrates. *Microbiology* **149**(9):2661-2667 DOI 10.1099/mic.0.26304-0.

668 **Greer-Phillips SE, Stephens BB, Alexandre G. 2004.** An energy taxis transducer promotes root colonization

669   by *Azospirillum brasilense*. *Journal of Bacteriology* **186**(19):6595-6604 DOI

670   10.1128/JB.186.19.6595-6604.2004.

671 **Guo M, Ye J, Gao D, Xu N, Yang J. 2019.** *Agrobacterium*-mediated horizontal gene transfer: Mechanism,

672   biotechnological application, potential risk and forestalling strategy. *Biotechnology Advances*

673   **37**(1):259-270 DOI 10.1016/j.biotechadv.2018.12.008.

674 **Guo M, Zhu Q, Gao D. 2009.** Development and optimization of method for generating unmarked *A.*

675   *tumefaciens* mutants. *Progress in Biochemistry and Biophysics* **36**(5):556-565 DOI

676   10.3724/Sp.J.1206.2008.00618.

677 **Hölscher T, Bartels B, Lin Y-C, Gallegos-Monterrosa R, Price-Whelan A, Kolter R, Dietrich LEP,**

678   **Kovács ÁT. 2015.** Motility, chemotaxis and aerotaxis Contribute to competitiveness during bacterial

679   pellicle biofilm development. *Journal of Molecular Biology* **427**(23):3695-3708 DOI

680   10.1016/j.jmb.2015.06.014.

681 **Hou S, Freitas T, Larsen RW, Piatibratov M, Sivozhelezov V, Yamamoto A, Meleshkevitch EA, Zimmer**

682   **M, Ordal GW, Alam M. 2001a.** Globin-coupled sensors: a class of heme-containing sensors in

683   Archaea and Bacteria. *Proceedings of the National Academy of Sciences of the United States of*

684   *America* **98**(16):9353-9358 DOI 10.1073/pnas.161185598.

685 **Hou S, Belisle C, Lam S, Piatibratov M, Sivozhelezov V, Takami H, Alam M. 2001b.** A globin-coupled

686   oxygen sensor from the facultatively alkaliphilic *Bacillus halodurans* C-125. *Extremophiles* **5**(5):351-

687   354 DOI 10.1007/s007920100220.

688 **Hou S, Larsen RW, Boudko D, Riley CW, Karatan E, Zimmer M, Ordal GW, Alam M. 2000.**

689   Myoglobin-like aerotaxis transducers in Archaea and Bacteria. *Nature* **403**(6769):540-544 DOI

690   10.1038/35000570.

691 **Huang Z, Wang YH, Zhu HZ, Andrianova EP, Jiang CY, Li D, Ma L, Feng J, Liu ZP, Xiang H, Zhulin**

692   **IB, Liu SJ. 2019.** Cross talk between chemosensory pathways that modulate chemotaxis and biofilm

693   formation. *mBio* **10**:e02876-18 DOI 10.1128/mBio.02876-18.

694 **Huang Z, Zhou Q, Sun P, Yang J, Guo M. 2018.** Two *Agrobacterium tumefaciens* CheW proteins are

695   incorporated into one chemosensory pathway with different efficiencies. *Molecular plant-microbe*

696   *interactions: MPMI* **31**(4):460-470 DOI 10.1094/MPMI-10-17-0255-R.

697 **Ichinose Y, Watanabe Y, Tumewu SA, Matsui H, Yamamoto M, Noutoshi Y, Toyoda K. 2023.**

698   Requirement of chemotaxis and aerotaxis in host tobacco infection by *Pseudomonas syringae* pv.

699   *tabaci* 6605. *Physiological and Molecular Plant Pathology* **124**:101970 DOI

700   10.1016/j.pmpp.2023.101970.

701 **Inoue H, Nojima H, and Okayama H. 1990.** High efficiency transformation of *Escherichia coli* with

702   plasmids. *Gene* **96**:23-28 DOI 10.1016/0378-1119(90)90336-p

703 **Jiang N, Liu W, Li Y, Wu H, Zhang Z, Alexandre G, Elmerich C, Xie Z. 2016.** A chemotaxis receptor

704   modulates nodulation during the *Azorhizobium caulinodans-Sesbania rostrata* symbiosis. *Applied and*

705   *Environmental Microbiology* **82**(11):3174-3184 DOI 10.1128/AEM.00230-16.

706 **Krell T, Lacal J, Muñoz-Martínez F, Reyes-Darias JA, Cadirci BH, García-Fontana C, Ramos JL. 2011.**

707   Diversity at its best: bacterial taxis. *Environmental Microbiology* **13**(5):1115-1124 DOI

708   10.1111/j.1462-2920.2010.02383.x.

709 **Kumar Verma R, Samal B, Chatterjee S. 2018.** *Xanthomonas oryzae* pv. *oryzae* chemotaxis components

710   and chemoreceptor Mcp2 are involved in the sensing of constituents of xylem sap and contribute to

711   the regulation of virulence-associated functions and entry into rice. *Molecular Plant Pathology*

712   **19**(11):2397-2415 DOI 10.1111/mpp.12718.

713 **Lang J, Faure D. 2014.** Functions and regulation of quorum-sensing in *Agrobacterium tumefaciens*. *Frontiers*

714   *in Plant Science* **5**:14 DOI 10.3389/fpls.2014.00014.

715 **Maschmann ZA, Chua TK, Chandrasekaran S, Ibáñez H, Crane BR. 2022.** Redox properties and PAS

716   domain structure of the *Escherichia coli* energy sensor Aer indicate a multistate sensing mechanism.

717   Journal of Biological Chemistry 298. DOI 10.1016/j.jbc.2022.102598

718 **Matveeva TV, Lutova LA. 2014.** Horizontal gene transfer from *Agrobacterium* to plants. *Frontiers in Plant*

719   *Science* **5**:326 DOI 10.3389/fpls.2014.00326.

720 **Meyer T, Renoud S, Vigouroux A, Miomandre A, Gaillard V, Kerzaon I, Prigent-Combaret C, Comte G,**

721   **Morera S, Vial L, Lavire C. 2018.** Regulation of hydroxycinnamic acid degradation drives

722   *Agrobacterium fabrum* lifestyles. *Molecular plant-microbe interactions: MPMI* **31**(8):814-822 DOI

723   10.1094/MPMI-10-17-0236-R.

724 **Păcurar DI, Thordal-Christensen H, Păcurar ML, Pamfil D, Botez C, Bellini C. 2011.** *Agrobacterium*

725   *tumefaciens*: From crown gall tumors to genetic transformation. *Physiological and Molecular Plant*

726   *Pathology* **76**(2):76-81 DOI 10.1016/j.pmpp.2011.06.004.

727 **Parkinson JS, Hazelbauer GL, Falke JJ. 2015.** Signaling and sensory adaptation in *Escherichia coli*

728   chemoreceptors: 2015 update. *Trends in Microbiology* **23**(5):257-266 DOI 10.1016/j.tim.2015.03.003.

729 **Perlova T, Gruebele M, Chemla YR, Mullineaux CW. 2019.** Blue light is a universal signal for *Escherichia*

730   *coli* chemoreceptors. *Journal of Bacteriology* **201**(11):e00762-18 DOI 10.1128/jb.00762-18.

731 **Rico-Jimenez M, Roca A, Krell T, Matilla MA. 2022.** A bacterial chemoreceptor that mediates chemotaxis

732   to two different plant hormones. *Environmental Microbiology* **24**(8): 3580-3597 DOI 10.1111/1462-

733   2920.15920.

734 **Rivera S, Young PG, Hoffer ED, Vansuch GE, Metzler CL, Dunham CM, Weinert EE. 2018.** Structural

735   insights into oxygen-dependent signal transduction within globin coupled sensors. *Inorganic*

736   *Chemistry* **57**(22):14386-14395 DOI 10.1021/acs.inorgchem.8b02584.

737 **Salah Ud-Din AIM, Roujeinikova A. 2017.** Methyl-accepting chemotaxis proteins: a core sensing element in

738   prokaryotes and archaea. *Cellular and Molecular Life Sciences* **74**(18):3293-3303 DOI

739   10.1007/s00018-017-2514-0.

740 **Shi K, Fan X, Qiao Z, Han Y, McDermott TR, Wang Q, Wang G. 2017.** Arsenite oxidation regulator AioR

741   regulates bacterial chemotaxis towards arsenite in *Agrobacterium tumefaciens* GW4. *Scientific reports*

742   **7**:43252 DOI 10.1038/srep43252.

743 **Stewart PS, Franklin MJ. 2008.** Physiological heterogeneity in biofilms. *Nature Reviews Microbiology*

744   **6**(3):199-210 DOI 10.1038/nrmicro1838.

745   **Sweeney E, Henderson JN, Goers J, Wreden C, Hicks KG, Foster JK, Parthasarathy R, Remington SJ,**

746   **Guillemin K. 2012.** Structure and proposed mechanism for the pH-sensing *Helicobacter pylori*

747   chemoreceptor TlpB. *Structure* **20**(7):1177-1188 DOI 10.1016/j.str.2012.04.021.

748   **Tumewu SA, Watanabe Y, Matsui H, Yamamoto M, Noutoshi Y, Toyoda K, Ichinose Y. 2022.**

749   Identification of aerotaxis receptor proteins involved in host plant infection by *Pseudomonas syringae*

750   pv. *tabaci* 6605. *Microbes and Environments* **37**(1): ME21076 DOI 10.1264/jsme2.ME21076.

751   **Vinogradov SN, Walz D A, Pohajdak B. 1992.** Organization of non-vertebrate globin genes. Comparative

752   *Biochemistry and Physiology Part B: Comparative Biochemistry* **103**(4): 759-773 DOI 10.1016/0305-

753   0491(92)90193-u.

754   **Walker JA, Rivera S, Weinert EE. 2017.** Mechanism and role of globin-coupled sensor signalling. *Advances*

755   *in Microbial Physiology* **71**:133-169 DOI 10.1016/bs.ampbs.2017.05.003.

756   **Wang H, Zhang M, Xu Y, Zong R, Xu N, Guo M. 2021.** *Agrobacterium fabrum* atu0526-encoding protein is

757   the only chemoreceptor that regulates chemoattraction toward the broad antibacterial agent formic

758   acid. *Biology (Basel)* **10**(12):1345**.** DOI 10.3390/biology10121345.

759   **Wood DW, Setubal JC, Kaul R, Monks DE, Kitajima JP, Okura VK, Zhou Y, Chen L, Wood GE,**

760   **Almeida NF, Jr., Woo L, Chen Y, Paulsen IT, Eisen JA, Karp PD, Bovee D, Sr., Chapman P,**

761   **Clendenning J, Deatherage G, Gillet W, Grant C, Kutyavin T, Levy R, Li MJ, McClelland E,**

762   **Palmieri A, Raymond C, Rouse G, Saenphimmachak C, Wu Z, Romero P, Gordon D, Zhang S,**

763   **Yoo H, Tao Y, Biddle P, Jung M, Krespan W, Perry M, Gordon-Kamm B, Liao L, Kim S,**

764   **Hendrick C, Zhao ZY, Dolan M, Chumley F, Tingey SV, Tomb JF, Gordon MP, Olson MV,**

765   **Nester EW. 2001.** The genome of the natural genetic engineer *Agrobacterium tumefaciens* C58.

766   *Science* **294**(5550):2317-2323 DOI 10.1126/science.1066804.

767   **Xie Z, Ulrich LE, Zhulin IB, Alexandre G. 2010.** PAS domain containing chemoreceptor couples dynamic

768   changes in metabolism with chemotaxis. *Proceedings of the National Academy of Sciences of the*

769   *United States of America* 107(5):2235-2240. DOI 10.1073/pnas.0910055107.

770   **Xu N, Wang M, Yang X, Xu Y, Guo M. 2020.** *In silico* analysis of the chemotactic system of *Agrobacterium*

771   *tumefaciens*. *Microbial Genomics* 6(11): mgen000460 DOI 10.1099/mgen.0.000460.

772   **Yang J, Pan X, Xu Y, Li Y, Xu N, Huang Z, Ye J, Gao D, Guo M. 2020.** *Agrobacterium tumefaciens*

773   ferritins play an important role in full virulence through regulating iron homeostasis and oxidative

774   stress survival. *Molecular Plant Pathology* **21**(9):1167-1178 DOI 10.1111/mpp.12969.

775   **Yao J, and Allen C. 2007.** The plant pathogen *Ralstonia solanacearum* needs aerotaxis for normal biofilm

776   formation and interactions with its tomato host. *Journal of Bacteriology* **189**(17):6415-6424 DOI

777   10.1128/jb.00398-07.

778   **Ye J, Gao M, Zhou Q, Wang H, Xu N, Guo M. 2021.** The only chemoreceptor encoded by *che* operon

779   affects the chemotactic response of *Agrobacterium* to various chemoeffectors. *Microorganisms*

780   **9**(9):1923 DOI 10.3390/microorganisms9091923.

781   **Zhulin IB, Bespalov VA, Johnson MS, Taylor BL. 1996.** Oxygen taxis and proton motive force in

782   *Azospirillum brasilense*. *Journal of Bacteriology* **178**(17):5199-5204 DOI 10.1128/jb.178.17.5199-

783   5204.1996.

784   **Zong R, Gao M, Zhang M, Wang H, Xu N, Guo M. 2022.** Functional identification of *Agrobacterium*

785   *tumefaciens* chemoreceptor MCP_{1912} in regulating chemotactic response. *Acta Microbiologica Sinica*

786   **62**(5):1949–1961 DOI 10.13343/j.cnki.wsxb.20210666.

Figure 1

Sequences and domain information of Atu1027.

(A) Domains of HemAT-Bs (*Bacillus subtilis*), HemAT-Hs (*Halobacterium salinarum*), and Atu1027 (*Agrobacterium tumefaciens*) predicted by Pfam and PROSITE servers. (B) Amino acid sequence alignment of globin domain of HemAT-Bs, HemAT-Hs, and Atu1027. The amino acid full alignment was created using the Clustal program of DNAman8 software. All settings used default values. The numbers on the right of the figure indicate the position of the amino acid. Asterisks signify the residues that are conserved across all globin domains, whereas the dark spots indicate residues that are highly conserved in all globin domains (*Bashford, Chothia & Lesk, 1987*; *Vinogradov et al., 1992*; *Hou et al., 2000*).

Figure 2

The interactions between Atu1027 and two CheWs.

(A) Bacterial two-hybrid assay. The *E. coli* cells co-expressing four combinations of target protein and bait protein were streaked on the X-gal indicator plate. The first combination is a positive control expressing LGF2 and Gal11, two proteins that are known to interact with each other; the second combination expresses Atu1027 and CheW1; the third combination expresses Atu1027 and CheW2; the fourth combination is a negative control expressing a single LGF2 protein. The interaction of the target protein and bait protein will activate the activity of β-galactosidase to catalyze the hydrolysis of X-gal, leading to the appearance of blue colonies. The chromogenic reaction of colonies harboring different combinations of target protein and bait protein are shown on the X-gal indicator plate. (B) Quantification of β-galactosidase activity of different combinations. The data represents the means ± standard deviations from three separate experiments, each with triplicate samples. Significant differences between groups are indicated by different letters on the bar ($P<0.05$). (C) The interactions between Atu1027 and two CheWs were tested using a His-tag pull-down assay. Initially, overproduced Atu1027-His and SalT-His were bound to the Ni-IDA resins individually, followed by the pull-down of overproduced CheW1 or CheW2. SalT-His was utilized as a negative control to confirm the specificity of Atu1027-His binding to CheWs. The original western blot image can be found in Supplementary Fig. S3.
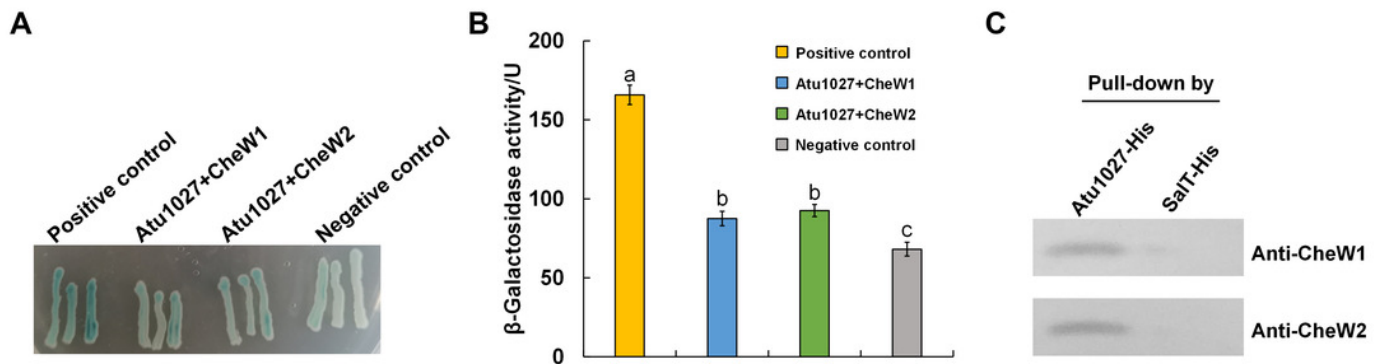
Figure 3

Air trap assays of wild-type C58, *atu1027*-deficient mutant C58Δ1027, and its complemented strain C58Δ1027+.

(A) A schematic of the air trap device. The device consists of a glass tube filled with AB-sucrose semi-solid medium, a Pasteur pipette, a rubber ring, and a lid made of aluminum foil. The glass tube was sterilized by autoclave with the Pasteur pipette. A rubber ring was tied to the upper end of the Pasteur pipette to keep it upright in the glass tube. To facilitate air diffusion and exchange, the Pasteur pipette's mouth was shaped into a pointed tip. 2 mL of the liquid paraffin was gently added to the medium, but not the Pasteur pipette. (B) Pictures represent bacterial behavior in the air trap device. If the air is detected by *A. tumefaciens* and acts as an attractant, the *A. tumefaciens* cells will move to the medium surface and gather at the favorable position inside the Pasteur pipette. The yellow arrows mark the position of the bacterial cells after incubation.

A
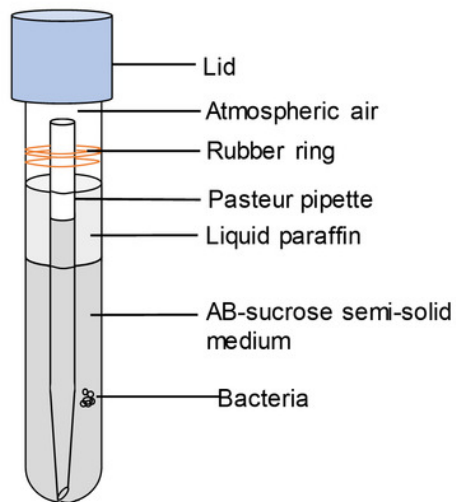
B
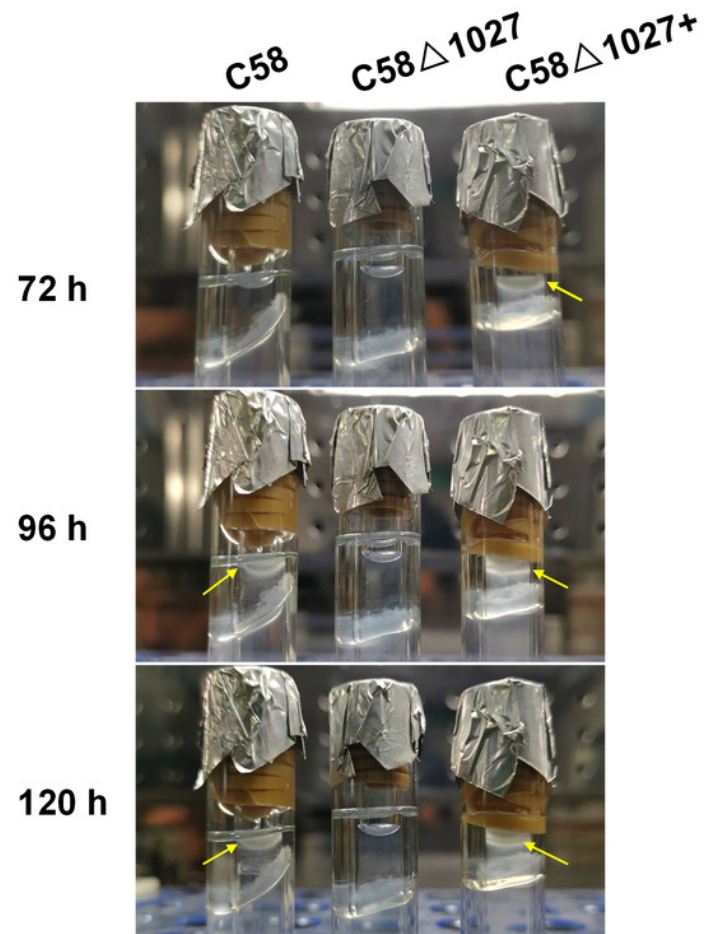
Figure 4

Bacterial aerotaxis behavior observation under the optical microscope.

In the experiment, middle-logarithmic *A. tumefaciens* strains were washed and suspended in a chemotaxis buffer with 14.6 mM sucrose for the energy supply. The coverslips were inverted over excavated slides after 2 μL of bacterial cells were deposited on the coverslip. This resulted in the air surrounding the drop. Then *A. tumefaciens* strains were observed under optical microscopy at 1000 × magnification. 5, 10, and 15 minutes after the droplets were dropped, photographs were taken of bacterial behavior at the edges of the droplets. Videos showing the bacterial response to atmospheric air were also provided in the supplementary material. Video S1: wild type C58; Video S2: C58Δ1027; Video S3: C58Δ1027+.

	5 min	**10 min**	**15 min**

C58

air
Drop edge
5 μm

C58△1027

air
Drop edge
5 μm

C58△1027+

air
Drop edge
5 μm
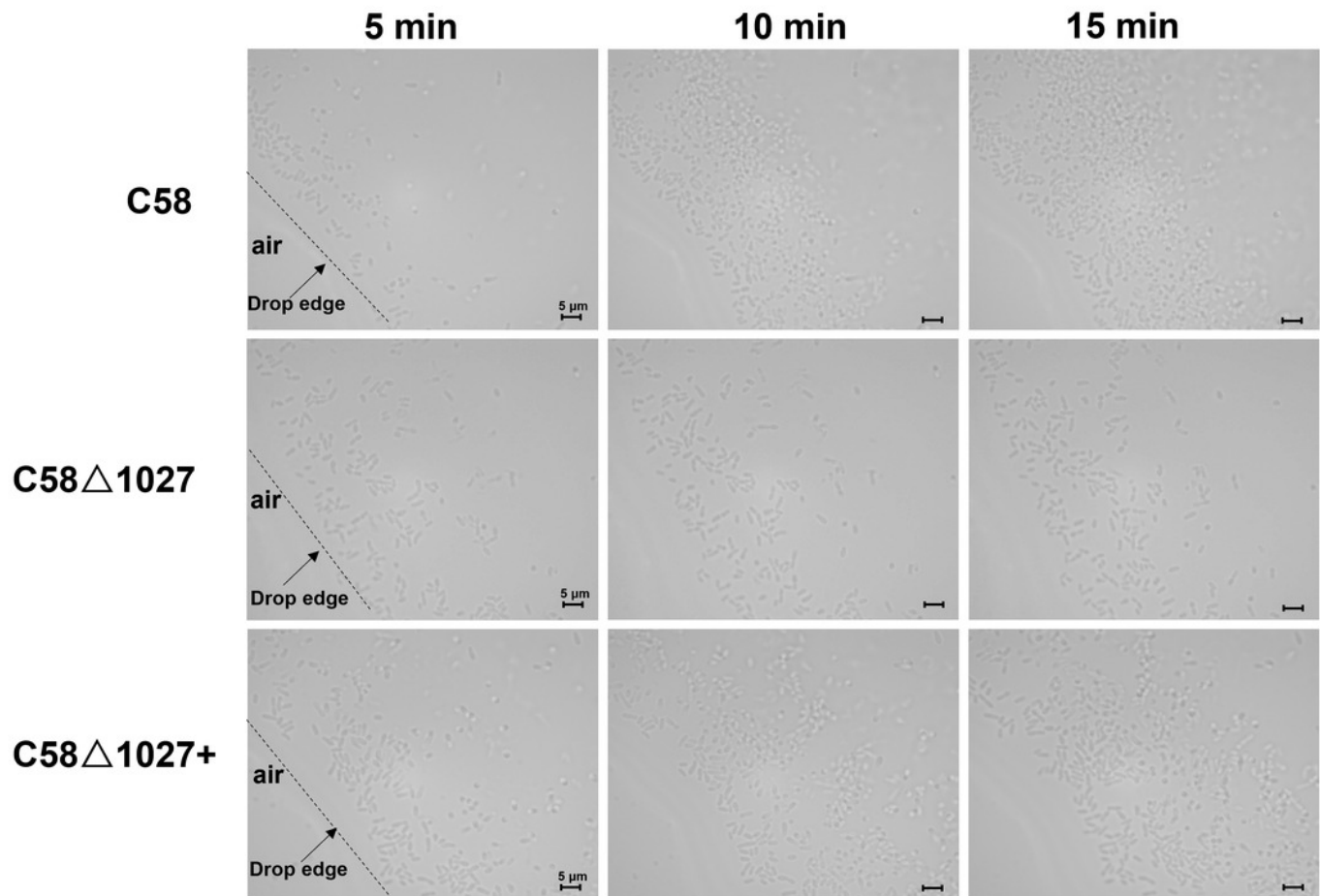
Figure 5

Comparison of chemotactic behavior between wild-type C58, *atu1027*-deficient mutant C58Δ1027, and its complemented strain C58Δ1027+.

Equal amounts of cells from different *A. tumefaciens* strains that were grown to the middle-log phase were inoculated on the swimming plates. The diameter of the bacterial colony after growing for 48 h on the swimming plate was used to quantify the chemotactic response of *A. tumefaciens* to six common carbon sources. (A) Typical colonies of different *A. tumefaciens* strains at 48 h post-inoculation on the swimming plate. (B) Statistical results of swimming halo diameter from different *A. tumefaciens* strains at 48 h post-inoculation on the swimming plate. The data are the means from four plates with standard errors. The letters above the bars represent significant differences obtained by one-way analysis of variance, followed by all pairwise multiple comparison procedures (SNK test) $p < 0.05$ (DPS software). C58, *A. tumefaciens* wild-type C58; C58Δ1027, *atu1027*-deficient mutant that derives from C58; C58Δ1027+, the complementation strain of C58Δ1027 carrying pCB301-C1027; C58Δ*w*, *cheW1-cheW2* double-deficient mutant deriving from C58 (as the chemotaxis-negative strain) (*Huang et al., 2018*)

A

mannitol

xylose

fructose

sucrose

glucose

galactose
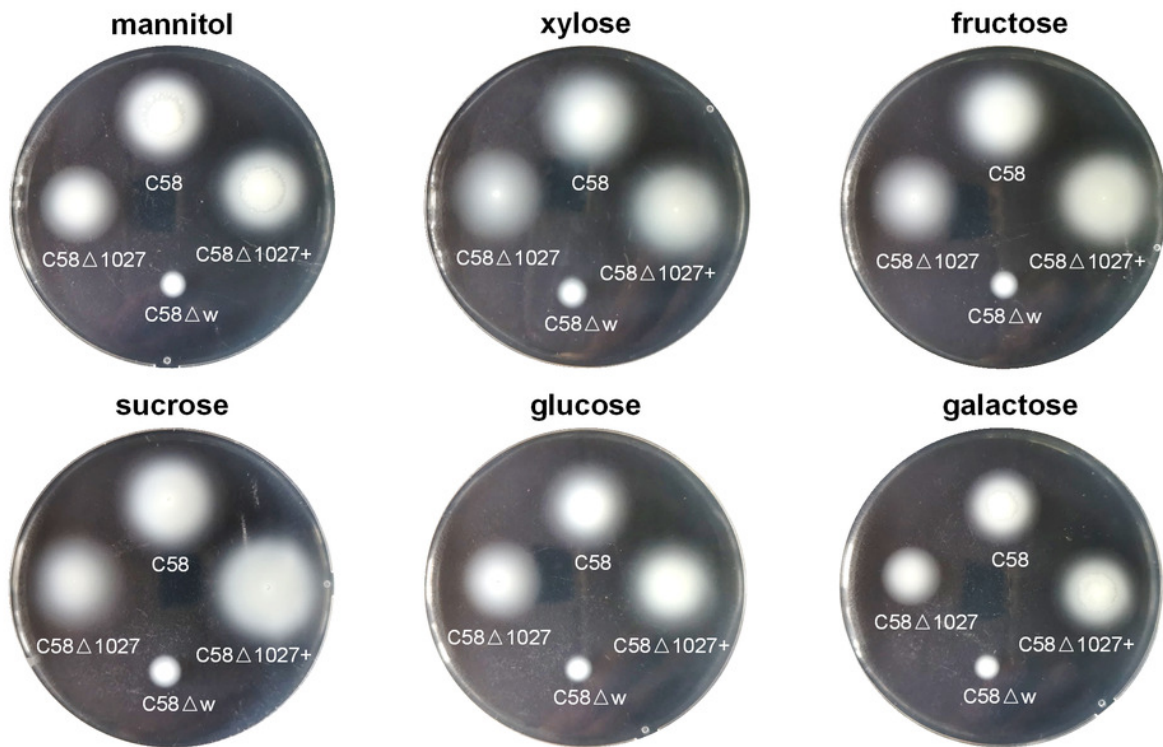
B
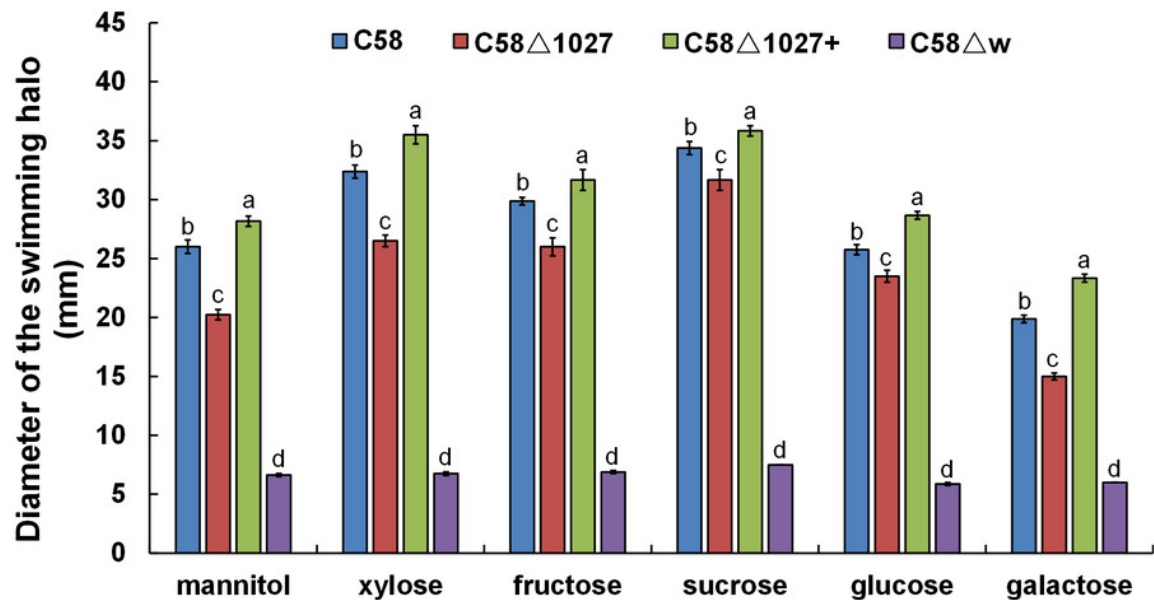
Figure 6

Effect of His100 within Atu1027 on chemotaxis and aerotaxis of *A. tumefaciens*.

The chemotaxis to sucrose and aerotaxis to atmospheric air was tested among wild-type C58, C58Δ1027, and C58Δ1027H100A. (A) The swimming plate containing sucrose as the carbon source shows typical swimming halos of C58, C58Δ1027, and C58Δ1027H100A on the swimming plate. (B) Statistical results of swimming halo diameter from C58, C58Δ1027, and C58Δ1027H100A at 48 h post-inoculation. (C) A typical photograph of bacterial aerotaxis in the air trap device at 120 h post-inoculation. Yellow arrows indicate the positions of the bacteria in the Pasteur pipette. In the bar graph, different letters indicate significant differences between groups (P<0.05).
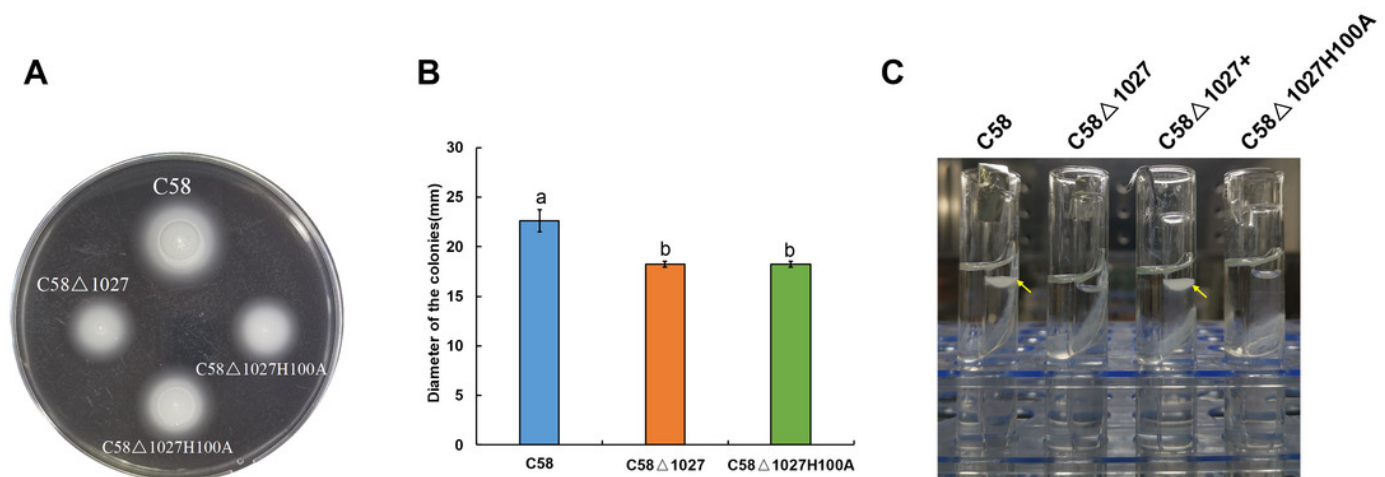
Figure 7

Biofilm formation of *A. tumefaciens* C58 and its Atu1027 mutant strains.

The biofilm formation of wild-type C58, C58Δ1027, and C58Δ1027+ was quantified by a crystal violet (CV) staining method. The OD570 value of the 30% acetic acid (vol/vol) - solubilized CV and the OD600 value of the planktonic cells were recorded and calculated. To exclude the influence of the growth rate of different strains on biofilm formation under static conditions, the ratio of OD570/OD600 was used to normalize the differences in culture growth between strains and to quantify the biofilm formation of C58, C58Δ1027, and C58Δ1027+. Different letters on the bar indicate significant differences between different groups (P<0.05).
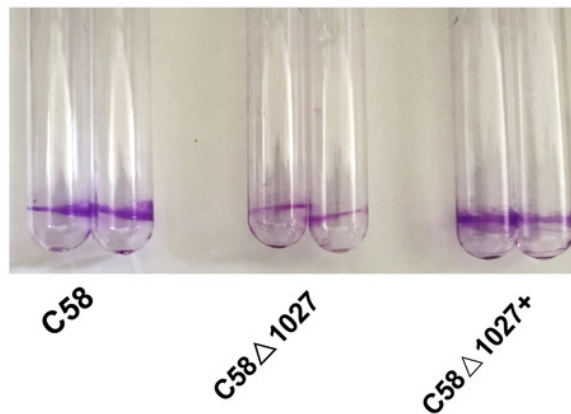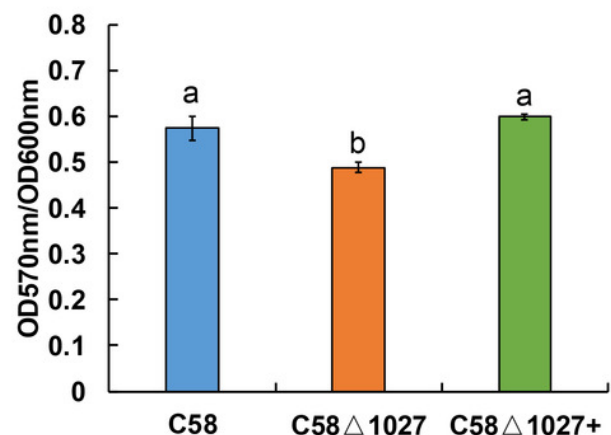
Figure 8

Tumorigenesis assays of *A. tumefaciens* C58 and its Atu1027 mutant strains.

Different *A. tumefaciens* strains were grown to the middle-log phase in AB-sucrose liquid medium. The cell concentration of all tested strains was adjusted to 5×10^8 cfu/mL. 3 μL cell suspension of different tested strains were respectively inoculated onto the wound lines on the leaves of *Kalanchoe* plants. An avirulent strain C58ΔvirA was used as a negative control. The *Kalanchoe* plants were grown at room temperature. The tumors on the leaves were photographed 30 days after inoculation. The tumors in each wound line were carefully scraped and weighted to quantify the pathogenicity. Data are the means of three biological replicates with the standard error. The letters above the bars represent significant differences obtained by one-way analysis of variance, followed by all pairwise multiple comparison procedures (SNK test) ($p < 0.05$).